

Effect of Alkali-Metal Additive on Rudorffite AgBiI₄-Based Pb-Free Solar Cells

Shanas Fatima,^{a,b} Dhruva B. Khadka,^{a†} Masatoshi Yanagida,^a Sunil Kumar Singh^b, Yasuhiro Shirai,^a

^a Photovoltaic Materials Group, Center for GREEN Research on Energy and Environmental Materials, National Institute for Materials Science (NIMS), 1-1 Namiki, Tsukuba, Ibaraki 305-0044, Japan

^bDepartment of Physics, Indian Institute of Technology (BHU) Varanasi, 221005, Uttar Pradesh, India

Corresponding Author

[†]e-mail: DBK: KHADKA.B.Dhruva@nims.go.jp

ABSTRACT

Rudorffite material, silver bismuth iodide, is one of the promising lead-free alternatives for photovoltaic applications due to its high absorption coefficient, low toxicity, and relatively better stability. Here, we report on the effects of alkali halide additive in the absorber material AgBiI₄, focusing on its material properties and solar cell devices. The inclusion of NaI significantly improved the film quality with compact and pinhole-free morphology and better crystallinity. The device with rudorffite material with NaI additive demonstrated a notable increase in the PCE from 1.33 to 3.72%, along with improved device stability. The device analysis confirmed that NaI incorporation in AgBiI₄ modulates the optoelectronic quality, effectively suppressing charge recombination and enhancing charge extraction within the device. Thus, this work corroborates that additive engineering is an effective strategy for improving both the efficiency and stability of AgBiI₄-based rudorffite solar cells, underscoring their potential in sustainable photovoltaic applications.

Keywords: lead-free, Ag-Bi-I system, rudorffite, additive, photovoltaic, defect passivation

1. INTRODUCTION

Halide perovskites have demonstrated a startling power conversion efficiency (PCE) of over 26 % for single-junction devices.^{1,2} Despite having such remarkable properties, the presence of toxic lead and instability towards moisture, air, and temperature is a major limitation.³⁻⁶ Exploring less toxic and stable absorber materials is crucial for developing effective lead-free alternatives. Sn and Ge, being members of the same group as Pb, are the first choices to substitute for Pb. Despite the lower toxicity of Ge and Sn, perovskites with Sn and Ge are relatively less stable in the ambient conditions due to the easy oxidation of Sn^{2+} and Ge^{2+} to Sn^{4+} and Ge^{4+} , respectively, and hence add challenges for photovoltaic applications.^{7,8} It is known that Bi^{3+} is relatively less toxic compared to Sn^{2+} .⁹ Furthermore, Bi^{3+} also shares a similar electronic configuration with Pb^{2+} i.e., $(6s^2 6p^0)$, making it an attractive alternative for developing bismuth-halide-based solar cells such as $\text{CH}_3\text{NH}_3\text{BiI}_4$, $\text{A}_3\text{Bi}_2\text{I}_9$ ($\text{A}=\text{Cs, Rb, K}$),^{10,11} $\text{Cs}_2\text{AgBiX}_6$ ¹²⁻¹⁴ etc. However, due to the indirect nature and wide bandgap of these materials, they are not feasible for single-junction solar cells.

Recently, ternary Ag-Bi-I materials have been explored as potential candidates for solar cell application as the light absorbing material due to their lower toxicity and relatively high stability against air and moisture.^{15,16} These silver bismuth iodides are known as rudorffites, having the general formula $\text{C}'\text{C}''\text{X}_2$, where both C' and C'' are sites in the cation sublattice with coordination no. 6, and X is a monovalent anion. C' and C'' form octahedra with the X, arranged alternately in the rudorffite structure. These octahedra do not share corners, unlike 3D halide perovskites.¹⁶ It has been reported that thermodynamically stable rudorffite materials such as Ag_3BiI_6 , Ag_2BiI_5 , AgBiI_4 , and AgBi_2I_7 , have potential in solar cell applications.¹⁶ The direct band gap of the silver iodo-bismuthates is approximately 1.8 eV, which is a suitable value for tandem solar cells.¹⁷ Sargent et al. reported a PCE of 1.22% with AgBi_2I_7 solar cell device having a band gap of 1.87 eV.¹⁸ Turkevych et al. have documented a detailed growth study of silver bismuth iodide as the absorbing material and reported a decent PCE of 4.3% with mesoporous and compact TiO_2 n-i-p configuration.¹⁶ Some reports documented compositional engineering with modulation of the electronic and photo-optical properties of Ag-Bi-I-based solar cells.^{19,20} To control the kinetics of film formation, regulating the dissolving process is important, like dissolving the precursors in one solvent or a mixture of solvents and various antisolvents that lead to different morphologies.^{21,22} Golobostanfard and coworkers reported solvent engineering for controlled crystal growth of rudorffite absorbers by varying the mixture composition of dimethylformamide (DMF) and dimethyl sulfoxide

(DMSO). Additionally, additive engineering is crucial for enhancing film quality by promoting crystallization and passivating defects. Multiple reports demonstrated that additive engineering, such as inorganic halide derivatives and functional molecular additives, benefits hybrid perovskites^{23–26} and rudorffites-based devices.^{27,28} Wang et al. reported an AgBiI₄ absorber layer incorporating Cs⁺ resulting in improved film quality and a PCE of 1.58%.²⁷ Functional additives such as Lewis base thiourea,²⁹ lithium bis(trifluoromethylsulfonyl)-imide,³⁰ etc, have also been reported to be beneficial for the improvement in AgBiI₄ solar cells. Despite multiple approaches, the efficiency of the Ag-Bi-I-based solar cell is quite low compared to the ideal value. This underscores the need for further advancements in material and transport engineering to achieve competitive performance in rudorffite-based solar cells.

In this work, we have investigated the effect of alkali halide additive on AgBiI₄, a bandgap of approximately 1.84 eV, as a Pb-free light-absorbing material. We examined the effect of Na⁺ ions on the morphology of the film and material chemistry. It was found that the film quality was significantly improved with well-covered and compact film surface morphology and ameliorated the surface chemistry for AgBiI₄ film with NaI additive. To evaluate the influence of additives, we fabricated solar cells with ITO/SnO₂/AgBiI₄-NaI/poly[bis(4-phenyl) (2,4,6-trimethylphenyl) amine] (PTAA)/Ag as n-i-p configuration. With the introduction of the Na⁺ additive, the PCE of the device was achieved as high as 3.72% with a significant increase in device parameters. This report has discussed an in-depth study of AgBiI₄, the thin film growth, and the photophysics of the device.

2. EXPERIMENTAL SECTION

2.1. Chemicals used

AgI (99.999%), BiI₃ (99%), Sodium iodide (NaI, 99.9%), dimethyl sulfoxide (DMSO), N, N-dimethylformamide (DMF), and poly[bis(4-phenyl)(2,4,6-trimethylphenyl)amine] (PTAA) purchased from Sigma-Aldrich, SnO₂ colloid (tin(IV) oxide) purchased from Alfa Aesar were used without any further purification. The FTO-coated and ITO-coated glasses purchased from Yingkou OPV Tech Co., Ltd were used throughout the deposition process.

2.2. Preparation of NaI: AgBiI₄ thin film and device

Preparation of precursor solution: A 0.6 M AgBiI₄ precursor solution was prepared by dissolving a 1:1 molar ratio of BiI₃ and AgI in (v/v) of 4:1 mixture of DMSO and DMF, followed by stirring at room temperature for 12 hours. For the NaI additive-based solution, different amounts of NaI (0.5, 1, 2 and 4 mg/ml) were added, which corresponds to 0.55, 1.11,

2.20 % and 4.46 mol % of NaI, respectively. These are written as 0, 0.5, 1, 2, and 4 mol % in the text for the sake of ease. The solutions were filtered by using a 0.22 μm pore-sized filter.

Spin coating ETL: Following a thorough cleaning, glass substrates coated with indium tin oxide (ITO) were exposed to UV ozone for 15 minutes. The SnO_2 colloid precursor (Alfa Aesar, 15% in H_2O colloidal dispersion) was diluted to 3% in distilled water. On the ITO substrates, a compact layer of SnO_2 was spin-coated for 30 seconds at 3000 rpm. This SnO_2 layer was annealed at 150 $^\circ\text{C}$ for 30 min in ambient air and cooled to room temperature.

Spin coating absorber layer: The SnO_2 -coated glasses were treated with UV-ozone for 30 min before the spin coating of the absorber (AgBiI_4 and NaI: AgBiI_4) layer. NaI additives (0.5, 1, 2, and 4) mol % in AgBiI_4 precursors were spin-coated at 1000 rpm for 10s (ramping slope 2 s) and 4000 rpm for 40 s followed by dripping 700 μl of isopropyl alcohol (IPA) at 33rd s of the second step and then the coated glasses were aged for 3 min before annealing at 100 $^\circ\text{C}$ for 15 min and 130 $^\circ\text{C}$ for 15 min.

Solar cell fabrication: The photovoltaic devices were fabricated on pre-cleaned patterned ITO-coated glass substrates. The ITO substrates were properly cleaned to remove organic residues, dust, and any unwanted impurities. First, the substrates were immersed in an ultrasonic bath with pure water, detergent, and 2-propanol, then treated with UV ozone for 5 minutes. After this, all the steps mentioned above were followed. PTAA was spin-coated after cooling the absorber layer-coated substrate to room temperature at 3000 rpm for 30 s (ramping slope 2) and then placed on the hot plate at 70 $^\circ\text{C}$ for 10 min. To complete the device structure, ~ 160 nm of Ag was thermally evaporated (at a pressure $<10^{-4}$ Pa).

2.3. Characterisations

The XRD patterns of all the NaI: AgBiI_4 films were taken by using Rigaku SmartLab ($\text{CuK } \alpha$ radiation, 1.54 \AA) at room temperature. The film morphology and various cross-section images were taken by high-resolution scanning electron microscope (SEM) at 5kV accelerating voltage (by Hitachi, S-4800). XPS spectra were obtained using a Versa Probe II (ULVAC-PHI, Japan). The thin films for XPS analysis were prepared inside an N_2 -filled glove box and transferred to the XPS chamber using an N_2 -filled transfer vessel to prevent oxygen contamination. The XPS measurements were conducted using a nonmonochromatic Al $\text{K}\alpha$ source (1486.6 eV) with a spot size ranging from 10 to 300 μm . A pass energy of 187.85 eV (1.5 eV step size) was used for the survey scan, while a pass energy of 46.95 eV (0.1 eV step size) was applied for the fine scan with a spot size of 100 μm . The spectra were calibrated using the binding energy of 284.8 eV for the C1s peak.

The absorption spectra of various films were measured using a UV–vis–NIR spectrometer (UV-2600i, Shimadzu). Emission spectra were collected by a micro-PL spectrometer (HORIBA, LabRamHR-PL NF(UV–NIR)) equipped with ≈ 532 nm laser diode (10 mW cm^{-2}) as an excitation source ($\lambda=420\text{nm}$) was used for obtaining the photoluminescence (PL) spectra. The carrier lifetimes were measured with a fluorescence lifetime spectrometer (Quantaaurus- τ from Hamamatsu-Photonics K.K., C11367) equipped with a ≈ 405 nm laser diode (typical peak power of 400 mW) at a 200 kHz repetition rate.

The J–V curves were measured at the scan rate of 0.05 V s^{-1} under one sun with an AM1.5G spectral filter (100 mW cm^{-2}) coupled with an MPPT system (System house Sunrise Corp.). The light intensity was calibrated by a silicon (Si) diode (BS-520BK). The external quantum efficiency (EQE) spectra were recorded using a spectrometer (SM-250 IQE, Bunkokeiki, Japan). The transient photovoltage was measured using a commercial PAIOS system (PAIOS V.4.3), with a pulse intensity applied to generate a photovoltage spike.

3. RESULTS AND DISCUSSION

3.1. Effect of Alkali Halide Additive on Rudorffite Film Growth and Material Properties

A schematic illustration for the preparation of AgBiI_4 films is depicted in Fig. 1a. The crystalline growth mechanism plays a crucial role in determining the film quality of AgBiI_4 . We investigated the effect of NaI additive on the surface morphology of the AgBiI_4 film by using scanning electron microscopy (SEM) images as given in Fig.1b-e, respectively. The control AgBiI_4 film (Fig. 1b) shows multiple pinholes, indicating a less compact microstructure. However, with the addition of NaI, the modified film displays a compact film with significantly fewer pinholes (to a pinhole-free morphology). This improvement suggests that NaI influences the crystallisation process of the absorber layer, leading to a more cohesive microstructure.^{31,32} The pinhole-free structure observed in the NaI-modified film is likely to enhance its photovoltaic performance, as a more compact surface could improve charge transport and reduce recombination losses. However, with an excessive amount of NaI, the film was more compact, and some whitish patches were observed, which could be due to the excess NaI on the film's surface. Moreover, compositional analysis (Table S1) using energy-dispersive X-ray spectroscopy (EDS) confirms that the stoichiometry of the precursors is the same as the precursor composition used, further suggesting that the absorber layer has a uniform composition. Interestingly, a slightly iodine-rich composition in AgBiI_4 film with additive was

observed, which could be due to additional iodine from the NaI additive. Elemental mapping (Fig. S1) shows a uniform distribution of NaI across the film surface.

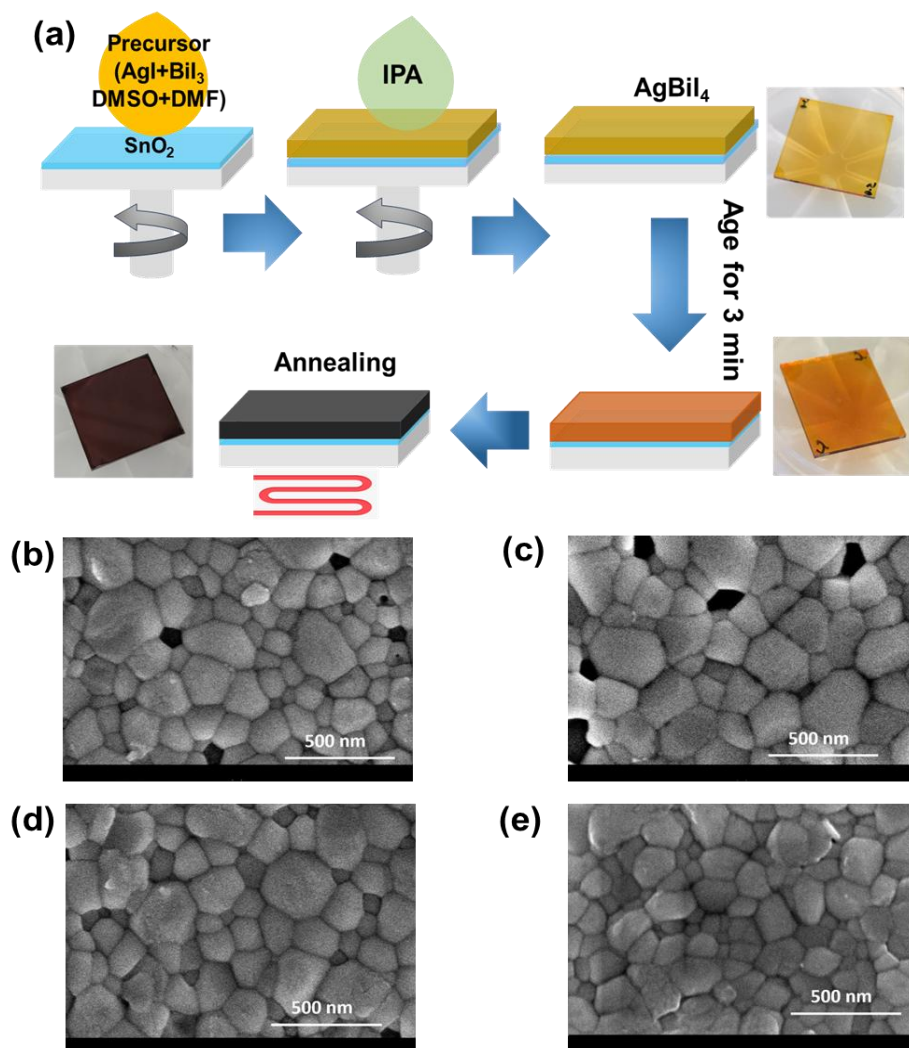


Figure 1. (a) Schematic of one-step spin coating for the preparation of AgBiI₄ films. Comparative SEM images of AgBiI₄ film with different concentrations of NaI additive: (b) 0, (c) ~0.5, (d) ~1, and (e) ~2 mol % of NaI, respectively.

To examine the effect of additives on the crystallinity of AgBiI₄ thin films, we measured X-ray diffraction (XRD) patterns. Figure 2a shows the XRD patterns for NaI-additive-based AgBiI₄ films with different NaI concentrations (0, 0.5, 1, 2, and 4 mol %). The dominant peak appears around $2\theta = 12.8^\circ$, corresponding to the (111) lattice plane, and other peaks at 21.57° , 23.8° , 29.31° , 30.65° , 38.98° , and 41.54° , which correspond to the (311), (222), (400), (331), (333), and (440) planes, respectively. These diffraction patterns are consistent with the cubic defect spinel structure.³³⁻²⁷ XRD patterns of NaI-additive-based films closely match with the control film, indicating crystal structure, and the phase remains intact. The dominant XRD peak (111)

shows the highest intensity at 2 mol % of NaI, with a minimal shift (Fig. S2a and Table S2). The diffraction peak of the (331) plane grows with increased NaI concentration in AgBiI₄ film. Importantly, the enhanced intensity of the dominant XRD peak and the decrease in the full width at half maxima (FWHM) (as summarised in Table S2 and shown in Fig S2b-f) with increasing NaI concentration implicates the improvement in crystallinity of AgBiI₄ film with NaI additive.

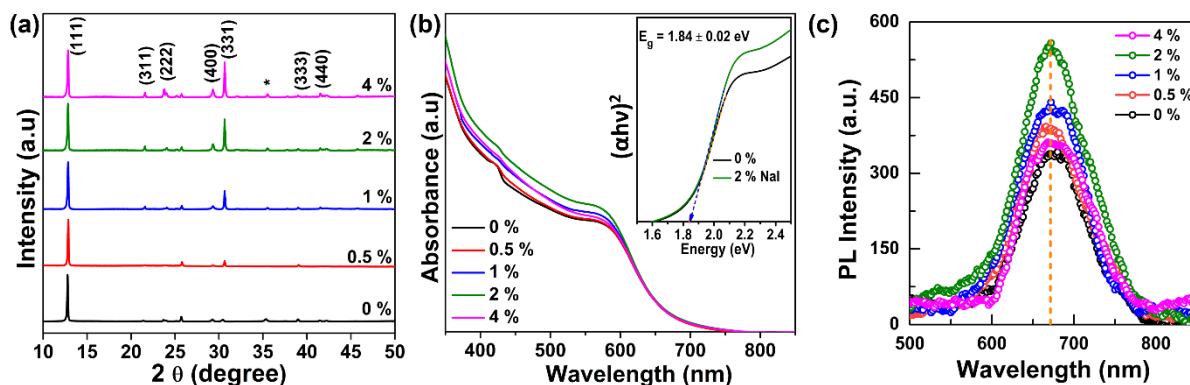


Figure 2. (a) XRD patterns. (* is the ITO peak) (b) UV-Vis spectra. (c) PL spectra of AgBiI₄ films with NaI additive (0, 0.5, 1, 2, and 4) mol %.

To study the effect of NaI additive on the optical properties, UV-Vis absorption spectra (Fig. 2b) were collected. AgBiI₄ exhibits notable absorption in the 360–750 nm range, making it a promising candidate for the absorber layer in solar cell applications. However, its overall absorption properties, like intensity and spectral range, are still inferior to Pb-based materials, which could potentially result in lower solar cell performance. AgBiI₄ films with varying NaI amounts show a slight increase in absorbance, while the absorbance onset at 580 nm remains unchanged. By using the Tauc analysis (inset Fig. 2b), the optical bandgap of both control and NaI additive-based AgBiI₄ films was estimated to be almost equal to 1.84 ± 0.02 eV, which is in agreement with the reported literature.^{16,29}

Moreover, we also collected steady-state PL spectra of the NaI additive-based AgBiI₄ films depicted in Fig 2c, and a comparative PL graph is shown in Fig S3. The observed slight increase in PL intensity indicates the improvement in the optoelectronic quality of AgBiI₄ films with NaI additive, which is consistent with the observed XRD patterns. The PL intensity enhancement in NaI-based films suggests defect passivation and decrement in non-radiative recombination.^{34,35} It is seen that the PL spectra of the control and additive-based AgBiI₄ films

are at almost the same peak position, centred around 672 nm ($\sim 1.84 \pm 0.02$ eV), as estimated from absorption spectra, indicating that the band edge of the AgBiI₄ is unaffected.

3.2. Photovoltaic Characteristic of NaI Additive-AgBiI₄ Solar Cells

To investigate the effects of NaI additive on the performance of AgBiI₄ rudorffite solar cells, we then fabricated devices with ITO/SnO₂/AgBiI₄/PTAA/Ag configuration as shown in schematic Fig. 3a and device cross-section SEM image (Fig. 3b). Figure 3c shows the J-V curves for the best control and NaI additive-based devices and figure of merits are given in (Table 1). The JV curve of the NaI additive-based device (Fig. 3c) demonstrates a reduced J-V hysteresis. The J-V curves of devices with different NaI concentrations (Fig. S4) and corresponding device parameters (Table S3) are given in the supporting information (SI). The device with NaI additive (2%) (hereafter, NaI additive device) demonstrated an optimal PCE of 3.72 % compared to the control device with a PCE of 1.33 %. Our result is among the best of the reported device performance of rudorffite-based solar cells, as listed in Table S4 and the plot shown in Fig. S5. This improvement was accompanied by a notable increase in all device parameters ($V_{OC} \sim 0.49$ to 0.58 V, $J_{SC} \sim 7.33$ to 10.74 mAcm⁻², and FF ~ 37.07 to 60.49 %), suggesting the passivation of traps and facilitation of effective carrier transport.³⁶

Table 1: Summary of device parameters obtained from the J-V curve analysis for control devices and devices with NaI additive.

| Device | J_{sc} (mA cm ⁻²) | V_{oc} (V) | FF (%) | PCE (%) | Average PCE (%) \pm SD |
|---------------------------|------------------------------------|-----------------|-------------|------------|-----------------------------|
| Control (0 mol%) | 7.33/6.94 | 0.49/0.46 | 37.07/30.84 | 1.33/0.9 | 1.19 ± 0.104 |
| NaI- additive (2 mol%) | 10.75/10.97 | 0.58/0.56 | 60.5/53.2 | 3.72/3.25 | 3.49 ± 0.147 |

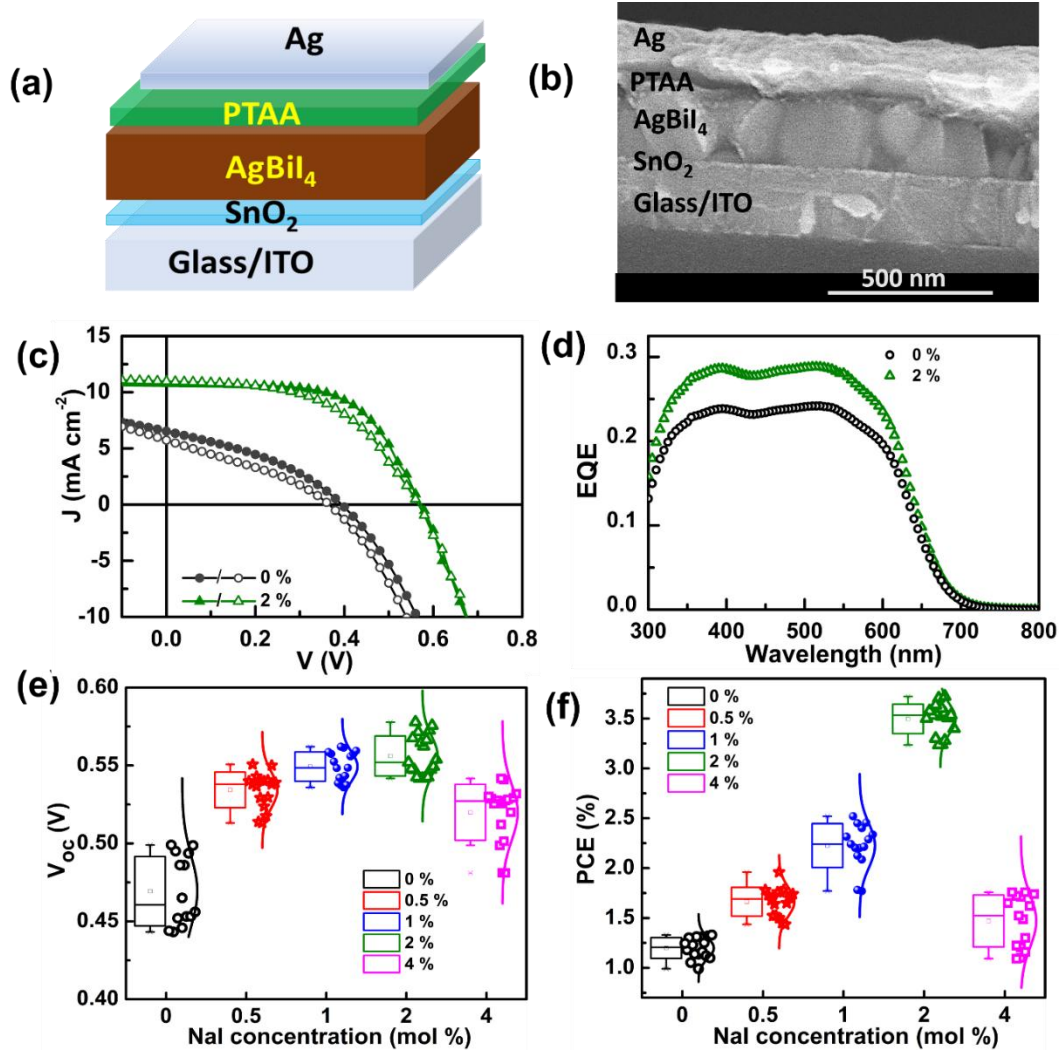


Figure 3. (a) Schematic and (b) cross-sectional SEM image of solar cell device with structure ITO/SnO₂/AgBiI₄/PTAA/Ag. (c) J - V curve and (d) EQE spectra of control and NaI-based solar cell device. (e) Statistics of PCE and (f) V_{OC} with varying NaI concentration. The error bars on each box indicate the minimum and maximum values, while the middle line represents the median. Small squares within the box denote the mean values.

To understand the spectral response, we have measured the external quantum efficiency (EQE) of the control and NaI additive devices (Fig. 3d). The AgBiI₄ device with NaI additive demonstrated overall enhancement in spectral response, suggesting improvement in both the bulk and interface quality with NaI additive as documented in Fujihara et al.^{37,38} The EQE spectral analysis (Fig. S6) yielded a bandgap of 1.84 ± 0.02 eV, which agrees with the bandgap estimated from the PL spectra and the absorption spectra.

To assess the relationship between alkali metal ion doping and photovoltaic performance, we conducted the statistical analysis of device parameters (V_{OC} , FF , J_{SC} , and PCE) of 15 devices with different NaI concentrations as depicted in Fig. 3e, f and SI (Fig. S7, Table S4). These statistical results display the trend of device parameters with different NaI additive concentrations. The standard deviation of device parameters has a lower value for the device with NaI additive, indicating higher reproducibility of device results compared to control devices. These results corroborate that the NaI additive in the AgBiI₄ device is beneficial for improvement in device performance as its reproducibility.

3.3. Effect of Additive on Transient Photo Characteristics and Defect Passivation

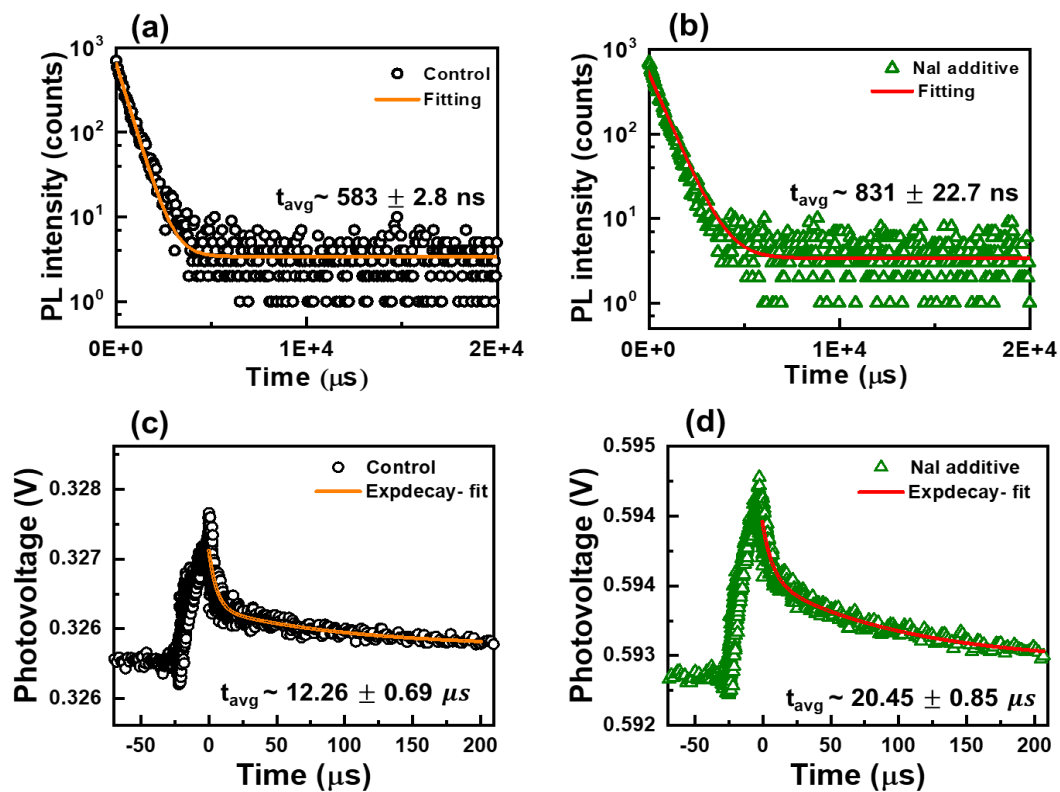


Figure 4. TRPL decay spectra of AgBiI₄-film (a) control and (b) with NaI additive. TPV curves of AgBiI₄-based devices (c) control and (d) with NaI.

To study the recombination dynamics and charge transport, we conducted time-resolved photoluminescence (TRPL) measurements. The TRPL spectra for AgBiI₄ films on ITO (Fig. 4a,b) and ITO/SnO₂ (Fig. S8) were analyzed to get the lifetime of photoexcited carriers. The decay time was calculated by using the single exponential function.^{39,40} The TRPL data of film

with NaI-additive (Fig. 4b) shows a longer PL lifetime (831 ns) compared to the control one (583 ns), indicating a mitigation of non-radiative recombination with NaI additive.^{41,42}

Furthermore, to investigate the transient photocarrier dynamic, we measured the transient photovoltage (TPV) characteristics for the control and NaI-additive devices by modulating V_{oc} with the transient illumination, as given in Fig. 4 (c-d). From the analysis of TPV decay curves, the NaI additive device showed a longer carrier lifetime ($\sim 20 \mu s$) compared to the control device ($\sim 12 \mu s$), suggesting a reduction in trap-assisted recombination.⁴³ These findings correlate with the enhanced performance of the NaI-based device, indicating defect passivation alongside other film characterisations.

3.4. Study of Surface Chemistry Modulation

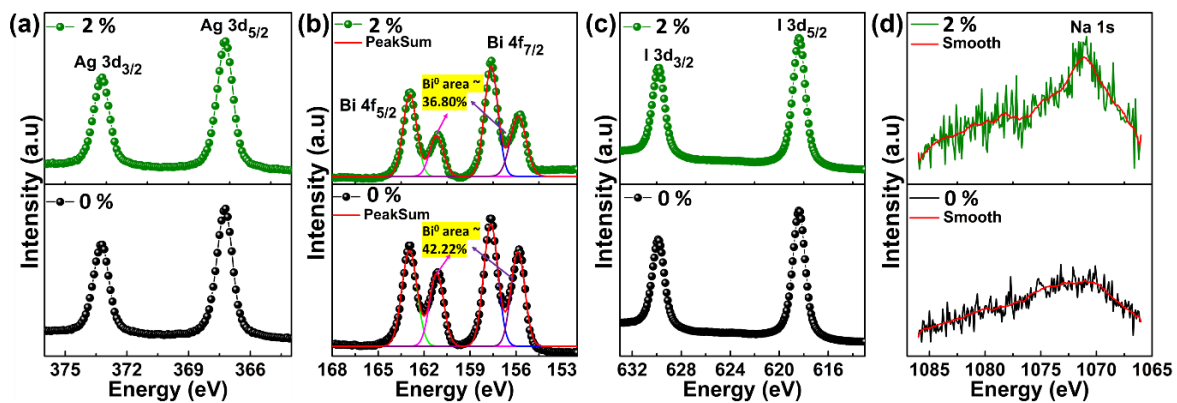


Figure 5. High-resolution XPS spectra of (a) Ag-3d, (b) Bi-4f, (c) I-3d, and (d) Na-1s core energy levels for AgBiI₄ (control) and NaI-additive AgBiI₄ films.

To further understand the surface chemistry of the synthesized films, X-ray photoelectron spectroscopy (XPS) analysis was conducted. The survey spectra of AgBiI₄ and NaI-incorporated AgBiI₄ are displayed in Fig. S9. A set of high-resolution XPS spectra for Ag-3d, Bi-4f, I-3d, and Na-1s are presented in Fig 5a-d. The Ag 3d core level (Fig. 5a) exhibits the characteristic peaks at 3d_{3/2} (375 eV) and 3d_{5/2} (369 eV), with no substantial shift in binding energies between control and NaI-additive AgBiI₄ film. However, in the case of Bi 4f spectra (Fig. 5b), XPS shoulder peaks at 162 eV (4f_{5/2}) and 156 eV (4f_{7/2}) align with the binding energies of metallic Bi⁰, appearing in both control and NaI-additive AgBiI₄ films as observed in previous reports.^{39,44,45} The metallic Bi⁰ is deleterious for film quality, which contributes to the reduction in efficiency and degradation. We found that metallic Bi⁰ peaks are suppressed

by 6 % in NaI-additive films (summarized in Table S5), implying that NaI addition enhances the interaction between Bi and I atoms. A similar observation has been documented for Ag_3BiI_6 film with the CuBr additive.⁴⁶ A decrease in metallic Bi may result from the interaction of Na with Bi atoms that are not integrated into the host crystal of the AgBiI_4 film. This interaction enhances surface chemistry, contributing to the improved performance of devices with the NaI additive. The I $3d_{3/2}$ and $3d_{5/2}$ characteristic peaks (Fig. 5c) are centered at binding energies of 631 and 619 eV, respectively. Due to the low concentration of NaI, the Na 1s peak appears with low intensity, as shown in Fig. 5d. These results corroborate that the NaI additive in AgBiI_4 film modulates film growth by regulating the morphology and ameliorating surface chemistry, which results in an improved device performance.

3.5. Impact of additive on device stability and film aging

Moreover, we examine the impact of the NaI additive on the stability of AgBiI_4 solar cells. The time-dependent PCEs of both control and NaI-treated devices are measured in air ambient (temperature: 50–55 °C; relative humidity: 30–40%) without any encapsulation, as shown in Fig. 6a. The control AgBiI_4 -based device retains 50% of its initial PCE after 20 h, whereas the NaI-based device retains 77% of its initial PCE after 30 h, showing better stability.

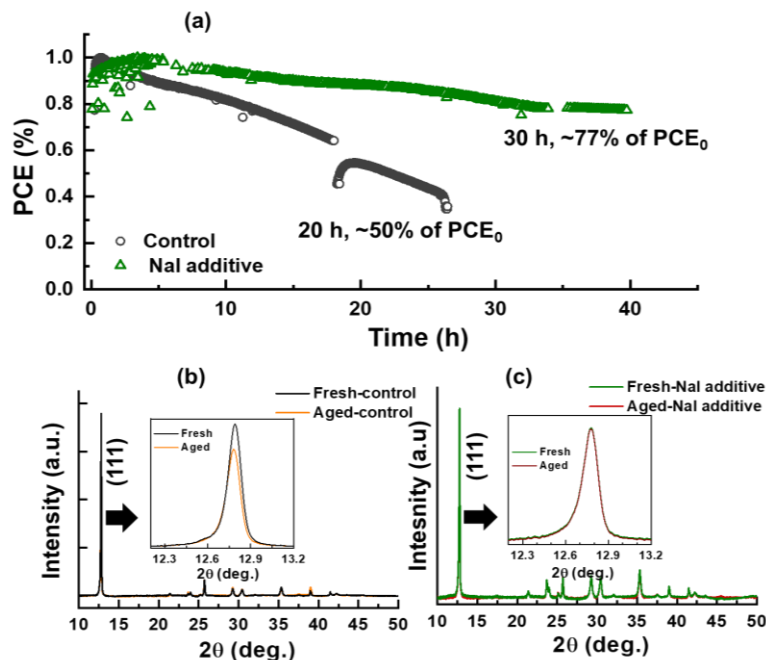


Figure 6. (a) Device stability plots of AgBiI_4 (control and NaI additive)- based solar cell devices. XRD patterns of fresh and aged AgBiI_4 film: (b) control and (c) NaI additive films with the inset of the zoomed (111) plane.

To assess the relation between the device and film stability, we also measured the XRD patterns (Fig. 6b, c) of the control film and NaI-additive film, respectively. XRD patterns of freshly prepared film and the aged film (30 days) were compared. Notably, no additional peaks appear in the aged XRD pattern for either the control or NaI-additive-based films, suggesting stable film with the absence of an additional secondary phase over time. A subtle change in the intensity of the dominant peak is observed. The control film shows a slight reduction in peak intensity, while the AgBiI₄ film with NaI additive almost remains unchanged, indicating that the NaI additive contributes to enhanced film stability. Additionally, the FWHM values for the peaks remain nearly identical between fresh NaI: AgBiI₄ (0.1084) and aged NaI: AgBiI₄ samples (0.1098), further supporting the stability of the AgBiI₄ absorber material under ambient conditions. Despite the structural stability of AgBiI₄, the observed decline in device efficiency over time suggests other potential degradation factors, such as interactions at the HTL and absorber interface.^{15,47,48}

4. CONCLUSIONS

We have investigated the effect of the alkali halide additive in Rudorffite AgBiI₄-based solar cells. The NaI additive regulates the crystallization of AgBiI₄ crystals and the formation of a highly compact and pinhole-free surface, leading to significantly improved AgBiI₄ film quality. The film with NaI additive also modulated the surface chemistry of AgBiI₄ film by quenching the metallic content of Bi⁰ ions, as confirmed by XPS analysis. The enhanced film quality led to a significant increase in PCE from 1.33 to 3.72 %, accompanied by improved device stability. The TRPL carrier lifetime increased substantially from 583 ns to 831 ns, indicating more efficient charge transfer, reduced defects, and suppressed carrier recombination, as supported by the TPV decay analysis. These findings highlight that additive engineering is a crucial approach to enhancing the efficiency and stability of AgBiI₄-based rudorffite solar cells.

ASSOCIATED CONTENT

Data Availability Statement

The data that support the findings of this study are available within the article.

Supporting Information

Supporting Information is available free of charge on the ACS website.

EDX mapping, XRD patterns analysis, PL spectra, J-V data, Device parameters table, Reported device data, Bandgap estimation, TRPL data, XPS spectra, Stability data.

Author Information

Corresponding author.

*Email: KHADKA.B.Dhruba@nims.go.jp (D.B.K.)

ORCID

Shanas Fatima: 0090-0000-8233-6277

Dhruba B. Khadka: 0000-0001-9134-3890

Masatoshi Yanagida: 0000-0002-8065-7875

Sunil Kumar Singh: 0000-0002-1028-6255

Yasuhiro Shirai: 0000-0003-2164-5468

Notes

The authors declare no competing financial interest.

Acknowledgments

This work was supported by The Hitachi Global Foundation, Kurata grants (#1572). Shanas Fatima is grateful to the National Institute for Materials Science (NIMS), Japan, and the Indian Institute of Technology (BHU), Varanasi, India, for the International Cooperative Graduate Program (ICGP) fellowship. SF is also thankful to the Ministry of Education for the Prime Minister Research Fellowship. The authors also acknowledge the technical support provided by Yamaguchi Kazuo-San (XPS) and Takahashi Hiromi (XRD) from the NIMS battery research platform for their respective measurement and analysis contributions. The authors are deeply thankful to Prof. Kenjiro Miyano for their insightful comments and constructive suggestions in this work.

References:

- (1) Green, M. A.; Dunlop, E. D.; Yoshita, M.; Kopidakis, N.; Bothe, K.; Siefert, G.; Hinken, D.; Rauer, M.; Hohl-Ebinger, J.; Hao, X. Solar Cell Efficiency Tables (Version 64). *Progress in Photovoltaics: Research and Applications* **2024**, 32 (7), 425–441.
- (2) Khadka, D. B.; Shirai, Y.; Yanagida, M.; Ryan, J. W.; Song, Z.; Barker, B. G.; Dhakal, T. P.; Miyano, K. Advancing Efficiency and Stability of Lead, Tin, and Lead/Tin Perovskite Solar Cells: Strategies and Perspectives. *Solar RRL* **2023**, 7 (21), 2300535. (3)
Saliba, M.; Stolterfoht, M.; Wolff, C. M.; Neher, D.; Abate, A. Measuring Aging Stability of Perovskite Solar Cells. *Joule* **2018**, 2 (6), 1019–1024.

- (4) Khadka, D. B.; Shirai, Y.; Yanagida, M.; Miyano, K. Insights into Accelerated Degradation of Perovskite Solar Cells under Continuous Illumination Driven by Thermal Stress and Interfacial Junction. *ACS Appl Energy Mater* **2021**, 4 (10), 11121–11132.
- (5) Khadka, D. B.; Yanagida, M.; Shirai, Y. Assessing Degradation in Perovskite Solar Cells via Thermal Hysteresis of Photocurrent and Device Simulation. *Solar Energy Materials and Solar Cells* **2025**, 281, 113319.
- (6) Lyu, M.; Yun, J.-H.; Chen, P.; Hao, M.; Wang, L. Addressing Toxicity of Lead: Progress and Applications of Low-Toxic Metal Halide Perovskites and Their Derivatives. *Adv Energy Mater* **2017**, 1602512.
- (7) Wang, F.; Ma, J.; Xie, F.; Li, L.; Chen, J.; Fan, J.; Zhao, N. Organic Cation-dependent Degradation Mechanism of Organotin Halide Perovskites. *Adv Funct Mater* **2016**, 26 (20), 3417–3423.
- (8) Khadka, D. B.; Shirai, Y.; Sahara, R.; Yanagida, M.; Miyano, K. Ameliorating Defects in Wide Bandgap Tin Perovskite Solar Cells Using Fluorinated Solvent and Hydrazide. *Small* **2024**, 2410048–2410048.
- (9) Huang, J.; Wang, H.; Jia, C.; Yang, H.; Tang, Y.; Gou, K.; Zhou, Y.; Zhang, D. High-Efficiency and Ultra-Stable Cesium–Bismuth-Based Lead-Free Perovskite Solar Cells without Modification. *J Phys Chem Lett* **2024**, 15 (12), 3383–3389.
- (10) Khadka, D. B.; Shirai, Y.; Yanagida, M.; Miyano, K. Tailoring the Film Morphology and Interface Band Offset of Caesium Bismuth Iodide-Based Pb-Free Perovskite Solar Cells. *J Mater Chem C Mater* **2019**, 7 (27), 8335–8343.
- (11) Jain, S. M.; Phuyal, D.; Davies, M. L.; Li, M.; Philippe, B.; De Castro, C.; Qiu, Z.; Kim, J.; Watson, T.; Tsoi, W. C.; Karis, O.; Rensmo, H.; Boschloo, G.; Edvinsson, T.; Durrant, J. R. An Effective Approach of Vapour Assisted Morphological Tailoring for Reducing Metal Defect Sites in Lead-Free, (CH₃NH₃)₃Bi₂I₉ Bismuth-Based Perovskite Solar Cells for Improved Performance and Long-Term Stability. *Nano Energy* **2018**, 49 (6), 614–624.
- (12) Slavney, A. H.; Hu, T.; Lindenberg, A. M.; Karunadasa, H. I. A Bismuth-Halide Double Perovskite with Long Carrier Recombination Lifetime for Photovoltaic Applications. *J Am Chem Soc* **2016**, 138 (7), 2138–2141.
- (13) Gao, W.; Ran, C.; Xi, J.; Jiao, B.; Zhang, W.; Wu, M.; Hou, X.; Wu, Z. High-Quality Cs₂AgBiBr₆ Double Perovskite Film for Lead-Free Inverted Planar Heterojunction Solar Cells with 2.2% Efficiency. *ChemPhysChem* **2018**, 19 (14), 1696–1700.
- (14) Igbari, F.; Wang, R.; Wang, Z.-K.; Ma, X.-J.; Wang, Q.; Wang, K.-L.; Zhang, Y.; Liao, L.-S.; Yang, Y. Composition Stoichiometry of Cs₂AgBiBr₆ Films for Highly Efficient Lead-Free Perovskite Solar Cells. *Nano Lett* **2019**, 19 (3), 2066–2073.
- (15) Kulkarni, A.; Ünlü, F.; Pant, N.; Kaur, J.; Bohr, C.; Jena, A. K.; Öz, S.; Yanagida, M.; Shirai, Y.; Ikegami, M.; Miyano, K.; Tachibana, Y.; Chakraborty, S.; Mathur, S.; Miyasaka, T. Concerted Ion Migration and Diffusion-Induced Degradation in Lead-Free Ag₃BiI₆ Rudorffite Solar Cells under Ambient Conditions. *Solar RRL* **2021**, 5 (8), 2100077.

- (16) Turkevych, I.; Kazaoui, S.; Ito, E.; Urano, T.; Yamada, K.; Tomiyasu, H.; Yamagishi, H.; Kondo, M.; Aramaki, S. Photovoltaic Rudorffites: Lead-Free Silver Bismuth Halides Alternative to Hybrid Lead Halide Perovskites. *ChemSusChem* **2017**, *10* (19), 3754–3759.
- (17) Eperon, G. E.; Leijtens, T.; Bush, K. A.; Prasanna, R.; Green, T.; Wang, J. T.-W.; McMeekin, D. P.; Volonakis, G.; Milot, R. L.; May, R.; Palmstrom, A.; Slotcavage, D. J.; Belisle, R. A.; Patel, J. B.; Parrott, E. S.; Sutton, R. J.; Ma, W.; Moghadam, F.; Conings, B.; Babayigit, A.; Boyen, H.-G.; Bent, S.; Giustino, F.; Herz, L. M.; Johnston, M. B.; McGehee, M. D.; Snaith, H. J. Perovskite-Perovskite Tandem Photovoltaics with Optimized Band Gaps. *Science (1979)* **2016**, *354* (6314), 861–865.
- (18) Kim, Y.; Yang, Z.; Jain, A.; Voznyy, O.; Kim, G.; Liu, M.; Quan, L. N.; García de Arquer, F. P.; Comin, R.; Fan, J. Z.; Sargent, E. H. Pure Cubic-Phase Hybrid Iodobismuthates AgBi₂I₇ for Thin-Film Photovoltaics. *Angewandte Chemie International Edition* **2016**, *55* (33), 9586–9590. (19) Jung, K. W.; Sohn, M. R.; Lee, H. M.; Yang, I. S.; Sung, S. Do; Kim, J.; Wei-Guang Diao, E.; Lee, W. I. Silver Bismuth Iodides in Various Compositions as Potential Pb-Free Light Absorbers for Hybrid Solar Cells. *Sustain Energy Fuels* **2018**.
- (20) Khazaei, M.; Sardashti, K.; Chung, C. C.; Sun, J. P.; Zhou, H.; Bergmann, E.; Dunlap-Shohl, W. A.; Han, Q.; Hill, I. G.; Jones, J. L.; Lupascu, D. C.; Mitzi, D. B. Dual-Source Evaporation of Silver Bismuth Iodide Films for Planar Junction Solar Cells. *J Mater Chem A Mater* **2019**, *7* (5), 2095–2105.
- (21) Ghosh, B.; Wu, B.; Guo, X.; Harikesh, P. C.; John, R. A.; Baikie, T.; Arramel; Wee, A. T. S.; Guet, C.; Sum, T. C.; Mhaisalkar, S.; Mathews, N. Superior Performance of Silver Bismuth Iodide Photovoltaics Fabricated via Dynamic Hot-Casting Method under Ambient Conditions. *Adv Energy Mater* **2018**, *8* (33), 1802051.
- (22) Zhai, W.; Huang, L.; Cui, X.; Li, G.; Zhang, Z.; Chen, P.; Li, Y.; Tang, Y.; Lin, L.; Yan, Z.; Liu, J.-M. Tuning the Morphology and Optoelectronic Properties of AgBiI₄ Film through Isopropanol Treatment. *J Mater Chem C Mater* **2022**, *10* (13), 5321–5327.
- (23) Lee, J.; Kim, D.; Kim, H.; Seo, S.; Cho, S. M.; Park, N. Formamidinium and Cesium Hybridization for Photo-and Moisture-stable Perovskite Solar Cell. *Adv Energy Mater* **2015**, *5* (20), 1501310.
- (24) Yi, C.; Luo, J.; Meloni, S.; Boziki, A.; Ashari-Astani, N.; Grätzel, C.; Zakeeruddin, S. M.; Röthlisberger, U.; Grätzel, M. Entropic Stabilization of Mixed A-Cation ABX₃ Metal Halide Perovskites for High Performance Perovskite Solar Cells. *Energy Environ. Sci.* **2016**, *9* (2), 656–662.
- (25) Khadka, D. B.; Shirai, Y.; Yanagida, M.; Miyano, K. Attenuating the Defect Activities with a Rubidium Additive for Efficient and Stable Sn-Based Halide Perovskite Solar Cells. *J Mater Chem C Mater* **2020**, *8* (7), 2307–2313.
- (26) Zhou, N.; Shen, Y.; Zhang, Y.; Xu, Z.; Zheng, G.; Li, L.; Chen, Q.; Zhou, H. CsI Pre-Intercalation in the Inorganic Framework for Efficient and Stable FACsPbI₃(Cl) Perovskite Solar Cells. *Small* **2017**, *13* (23), 1700484.

- (27) Yu, F.; Wang, L.; Ren, K.; Yang, S.; Xu, Z.; Han, Q.; Ma, T. Cs-Incorporated AgBiI₄ Rudorffite for Efficient and Stable Solar Cells. *ACS Sustain Chem Eng* **2020**, *8* (27), 9980–9987.
- (28) Zhai, W.; Zheng, W.; Shi, P.; Huang, L.; Cui, X.; Chen, P.; Tang, Y.; Lin, L.; Yan, Z.; Liu, J.-M. Performance Improvement of AgBiI₄ Solar Cells by a Lewis Base Thiourea Additive. *The Journal of Physical Chemistry C* **2024**, *128* (20), 8154–8160.
- (29) Zhai, W.; Zheng, W.; Shi, P.; Huang, L.; Cui, X.; Chen, P.; Tang, Y.; Lin, L.; Yan, Z.; Liu, J.-M. Performance Improvement of AgBiI₄ Solar Cells by a Lewis Base Thiourea Additive. *The Journal of Physical Chemistry C* **2024**, *128* (20), 8154–8160.
- (30) Zhang, Q.; Wu, C.; Qi, X.; Lv, F.; Zhang, Z.; Liu, Y.; Wang, S.; Qu, B.; Chen, Z.; Xiao, L. Photovoltage Approaching 0.9 v for Planar Heterojunction Silver Bismuth Iodide Solar Cells with Li-TFSI Additive. *ACS Appl Energy Mater* **2019**, *2* (5), 3651–3656.
- (31) Bag, S.; Durstock, M. F. Large Perovskite Grain Growth in Low-Temperature Solution-Processed Planar p-i-n Solar Cells by Sodium Addition. *ACS Appl Mater Interfaces* **2016**, *8* (8), 5053–5057.
- (32) Okamoto, Y.; Sumiya, M.; Suzuki, Y. Perovskite Solar Cells with 19% Efficiency Achieved by an Advanced Three-Step Method Using Additional HC(NH₂)₂I–NaI Spin-Coating. *ACS Appl Energy Mater* **2019**, *2* (3), 1823–1831.
- (33) Oldag, T.; Aussieker, T.; Keller, H.-L.; Preitschaft, C.; Pfitzner, A. Solvothermale Synthese Und Bestimmung Der Kristallstrukturen von AgBiI₄ Und Ag₃BiI₆. *Z Anorg Allg Chem* **2005**, *631* (4), 677–682.
- (34) Khadka, D. B.; Shirai, Y.; Yanagida, M.; Masuda, T.; Miyano, K. Enhancement in Efficiency and Optoelectronic Quality of Perovskite Thin Films Annealed in MAOI Vapor. *Sustain Energy Fuels* **2017**, *1* (4), 755–766.
- (35) Jiang, Q.; Zhao, Y.; Zhang, X.; Yang, X.; Chen, Y.; Chu, Z.; Ye, Q.; Li, X.; Yin, Z.; You, J. Surface Passivation of Perovskite Film for Efficient Solar Cells. *Nat Photonics* **2019**, *13* (7), 460–466.
- (36) Leijtens, T.; Eperon, G. E.; Barker, A. J.; Grancini, G.; Zhang, W.; Ball, J. M.; Kandada, A. R. S.; Snaith, H. J.; Petrozza, A. Carrier Trapping and Recombination: The Role of Defect Physics in Enhancing the Open Circuit Voltage of Metal Halide Perovskite Solar Cells. *Energy Environ. Sci.* **2016**, *9* (11), 3472–3481.
- (37) Nakane, A.; Tampo, H.; Tamakoshi, M.; Fujimoto, S.; Kim, K. M.; Kim, S.; Shibata, H.; Niki, S.; Fujiwara, H. Quantitative Determination of Optical and Recombination Losses in Thin-Film Photovoltaic Devices Based on External Quantum Efficiency Analysis. *J Appl Phys* **2016**, *120* (6), 064505.
- (38) Khadka, D. B.; Shirai, Y.; Yanagida, M.; Tadano, T.; Miyano, K. Interfacial Embedding for High-Efficiency and Stable Methylammonium-Free Perovskite Solar Cells with Fluoroarene Hydrazine. *Adv Energy Mater* **2022**, *12* (38), 2202029.
- (39) Pandian, M. G. M.; Khadka, D. B.; Shirai, Y.; Umedov, S.; Yanagida, M.; Subashchandran, S.; Grigorieva, A.; Miyano, K. Effect of Solvent Vapour Annealing on Bismuth Triiodide

Film for Photovoltaic Applications and Its Optoelectronic Properties. *J Mater Chem C Mater* **2020**, *8* (35), 12173–12180.

- (40) Khadka, D. B.; Shirai, Y.; Yanagida, M.; Ota, H.; Lyalin, A.; Taketsugu, T.; Miyano, K. Defect Passivation in Methylammonium/Bromine Free Inverted Perovskite Solar Cells Using Charge-Modulated Molecular Bonding. *Nat Commun* **2024**, *15* (1), 882.
- (41) Jeon, B.-C.; Kim, J.; Moon, T. Effects of Br Substitution on Inorganic Rudorffite AgBiI₄ for Stable, Pb-Free Solar Cells. *ChemistrySelect* **2024**, *9* (22), e202400337.
- (42) Lu, C.; Zhang, J.; Sun, H.; Hou, D.; Gan, X.; Shang, M.; Li, Y.; Hu, Z.; Zhu, Y.; Han, L. Inorganic and Lead-Free AgBiI₄ Rudorffite for Stable Solar Cell Applications. *ACS Appl Energy Mater* **2018**, *1* (9), 4485–4492.
- (43) Sandberg, O. J.; Tvingstedt, K.; Meredith, P.; Armin, A. Theoretical Perspective on Transient Photovoltage and Charge Extraction Techniques. *The Journal of Physical Chemistry C* **2019**, *123* (23), 14261–14271. .
- (44) Li, T.; Hu, Y.; Morrison, C. A.; Wu, W.; Han, H.; Robertson, N. Lead-Free Pseudo-Three-Dimensional Organic–Inorganic Iodobismuthates for Photovoltaic Applications. *Sustain Energy Fuels* **2017**, *1* (2), 308–316.
- (45) Park, J. W.; Lim, Y.; Doh, K.-Y.; Jung, M. T.; Jeon, Y. I.; Yang, I. S.; Choi, H.; Kim, J.; Lee, D.; Lee, W. I. Enhancement of the Photovoltaic Properties of Ag₂BiI₅ by Cu Doping. *Sustain Energy Fuels* **2021**, *5* (5), 1439–1447. <https://doi.org/10.1039/D0SE01563F>.
- (46) Mutlu, A.; Zafer, C. Minimization of Metallic Bi⁰ Species to Increase the Efficiency and Stability of Ag₃BiI₆ Solar Cells via Cu Doping. *Solar Energy* **2022**, *234*, 190–202.
- (47) Khadka, D. B.; Shirai, Y.; Yanagida, M.; Uto, K.; Miyano, K. Analysis of Degradation Kinetics of Halide Perovskite Solar Cells Induced by Light and Heat Stress. *Solar Energy Materials and Solar Cells* **2022**, *246*, 111899.
- (48) Gueye, I.; Shirai, Y.; Khadka, D. B.; Seo, O.; Hiroi, S.; Yanagida, M.; Miyano, K.; Sakata, O. Chemical and Electronic Investigation of Buried NiO 1–δ/PCBM, and PTAA/MAPbI₃–XCl_x Interfaces Using Hard X-Ray Photoelectron Spectroscopy and Transmission Electron Microscopy. *ACS Appl Mater Interfaces* **2021**, *13* (42), 50481–50490.

TOC Graphics

This study demonstrates that the metal cation halide additive improves the nucleation and crystallization process of AgBiI₄ film, leading to a compact and pinhole-free film. The device efficiency increases from 1.33% to 3.72%. This enhancement is attributed to the mitigation of metallic Bi⁰ and the decrement in defects, which lead to more charge carriers.

